Journal of Food Engineering 188 (2016) 50–57

Contents lists available at ScienceDirect

Journal of Food Engineering

journal homepage: www.elsevier.com/locate/jfoodeng

# X-ray microtomography provides new insights into vacuum impregnation of spinach leaves

Valentina Panarese [a, b], Els Herremans [c], Dennis Cantre [c], Eda Demir [a, d], Antânio Vicente [e], Federico Gãmez Galindo [a, *], Bart Nicolai [c], Pieter Verboven [c]

[a] Food Technology, Engineering and Nutrition, Lund University, PO Box 124, SE 221 00, Lund, Sweden
[b] Food Science, Alma Mater Studiorum, University of Bologna, Piazza Goidanich 60, 47521 Cesena (FC), Italy
[c] Postharvest Group/Flanders Centre of Postharvest Technology, Division BIOSYST-MeBioS, University of Leuven, PO Box 2428, B-3001, Leuven Heverlee, Belgium
[d] Optifreeze AB, Skiffervägen 12, SE-22478, Lund, Sweden
[e] Centre of Biological Engineering, University of Minho, Campus de Gualtar, 4710-057 Braga, Portugal

ARTICLE INFO

*Article history:*
Received 11 February 2016
Received in revised form
5 April 2016
Accepted 13 May 2016

*Keywords:*
Microstructure
Porosity
*Spinacia oleracea*

ABSTRACT

Vacuum impregnation is used in the food industry to facilitate the impregnation of porous products with, e.g. firming, antioxidant, antimicrobial or cryoprotective agents. X-ray micro-tomography (μCT) was used to study the process of vacuum impregnation in spinach leaves. Low (300 mbar absolute pressure) and mild vacuum (150 mbar absolute pressure) impregnation protocols were used to impregnate an isotonic solution of trehalose in the leaves and μCT was used to make observations of the cross section of the impregnated samples and quantify their porosity. Results revealed that the free volume in the spongy mesophyll is easier to impregnate than the spaces around the palisade mesophyll. The low vacuum impregnation protocol provoked less impregnation close to the edge of the leaf than in its centre, probably accounting for an influence of the tissue structure on impregnation. The vacuum impregnation protocols tested in this investigation drastically decreased the proportion of large pores (>100 μm) and increased the proportion of small pores (<50 μm). The mild vacuum impregnation protocol, which was designed on the basis of measured apparent porosity, did not achieve full impregnation of the tissue.


## 1. Introduction

Vacuum impregnation (VI) of a porous tissue involves the removal of the gas normally contained in open pores and its replacement with a liquid. VI is used in the food industry to facilitate the impregnation of various products with, e.g. firming, antioxidant, antimicrobial or cryoprotective agents (Hironaka et al., 2011; Phoon et al., 2008; Barrera et al., 2009; Gras et al., 2003). In a VI process, porous products are immersed in a solution of different compositions and/or concentrations and subjected to a two-step pressure change. The first step (vacuum increase) consists on the reduction of the pressure in a solid-liquid system. During this step, the gas in the product pores is expanded and partially flows out until mechanical equilibrium is achieved. When the atmospheric pressure (second step) is restored, the residual air in the pores compresses and the external liquid flows into the pores due to the action of a hydrodynamic mechanism (HDM) (Fito et al., 1996; Fito, 1994; Fito and Pastor, 1994). The filling of the pores is affected by capillary pressure which depends on pore size, surface tension of the liquid and wetting angle between the liquid and the pore walls (Tylewicz et al., 2012). The pressure changes can also promote deformation (that could provoke an increase of volume) of the product due to viscoelastic properties of its solid matrix (deformation-relaxation phenomena, DRP) (Carciofi et al., 2012; Salvatori et al., 1997; Fito et al., 1996).

The complicated network of highly interconnected intercellular air spaces consisting of tortuous paths and clusters contributes to both anisotropy and heterogeneity of the tissue. Tylewicz et al. (2012) suggested that the flow of the impregnated liquid in the tissue is strongly influenced by the topology and geometry of this network. Using gas in scattering media absorption spectroscopy (GASMAS), these authors found that apples in which air was not totally exhausted during impregnation keep an internal reduced pressure which rises slowly towards ambient temperature over a

* Corresponding author.
*E-mail address:* federico.gomez@food.lth.se (F. Gãmez Galindo).

http://dx.doi.org/10.1016/j.jfoodeng.2016.05.013
0260-8774/

time scale of hours after the operation is terminated. This finding suggests that, in the case of apple parenchyma, the interconnected air spaces expose at least in part an essentially hydrophobic surface and the Laplace pressure term in Fito's model can be locally negative. The liquid flow will be arrested if the liquid interface arrives to a pore so narrow that the driving pressure would not overcome the capillary pressure. Therefore, pressure equilibration can only be achieved either by gas diffusion in gas phase or by gradual wetting of the pores.

During vacuum impregnation, the liquid will convectively penetrate into the pores at a time scale given by pore sizes, the driving pressure difference and liquid viscosity. Fito and Chiralt (2000) calculated that the time scale for liquid flooding of apple air space is of the order of 1 s for a low viscosity liquid. This time scale was confirmed by the *in situ* time lapse microscopy results published by Panarese et al. (2013) where the impregnation of apple tissue was seen as soon as the restoration of the atmospheric pressure was started. These microscopic observations were also performed in spinach leaves, where impregnation occurred later. The difference between the impregnation of both materials was attributed to their different microstructure, pore size and wetting angle.

Impregnation might not be homogeneous in the heterogeneous matrix of the plant tissue due to differences in pore size distribution, morphology and porosity. These differences in impregnation have been confirmed by high resolution X-ray microtomography (μCT). Schulze et al. (2012) reported that VI resulted in a higher isotonic solution uptake in samples of the inner apple cortex compared to the outer part. Smaller cells and lower connectivity of intercellular spaces were attributed to be the cause of the lower impregnation results.

μCT is a non-destructive imaging technology to scrutinize the internal structures of plant tissues and characterize their 3D microstructure at the level of single cells and pores, determining size and shape distributions (Verboven et al., 2015; Herremans et al., 2013). The objective of this paper was to measure the 3D microstructural changes due to impregnation of spinach leaves and on the resulting tissue porosity.

## 2. Materials and methods

### 2.1. Raw material handling and storage

Locally grown baby spinach (*Spinacia oleracea* cv. Gazzelle) was harvested, washed, packed in 5 kg bags and transported to our laboratory within two hours after harvesting. Three hundred grams of spinach leaves (55 ± 5 mm of length) were packed in 30 × 30 cm OPPE, heat-sealed, laser perforated bags and stored at 4 °C until used in experiments which were performed within 3 days.

### 2.2. Impregnating solution

An isotonic solution in equilibrium with spinach leaves was designed with respect to the cell sap. The isotonic solution concentration was determined by immersing three spinach leaves (without petioles) in a series of solutions of different trehalose concentrations, according to Tylewicz et al. (2013). The variation of tissue weight was recorded every 30 min until equilibrium.

### 2.3. Apparent porosity

The pycnometer method described by Gras et al. (2002) was used to determine the spinach apparent density ($\rho_a$, in Kg m$^{-3}$) and the real solid-liquid density ($\rho_r$, in Kg m$^{-3}$). The apparent density was measured in leaf pieces by volume displacement in a pycnometer using the respective aqueous isotonic solution as reference liquid. The real solid-liquid density was also obtained by volume displacement, but in this case in samples purees, obtained by manually mashing the leaf samples using a mortar and pestle. The purees were degasified for 10 min by applying vacuum using a manual water pump. The total apparent porosity of the sample ($\varepsilon$) is the ratio of the apparent density and the real solid-liquid density (Eq. (1)) (Lozano et al., 1980):

$$\varepsilon = \left(1 - \frac{\rho_a}{\rho_r}\right) \times 100 \quad (1)$$

### 2.4. Vacuum impregnation

Vacuum impregnation was carried out at room temperature (20 ± 2 °C) in a chamber connected to a vacuum pump (PIAB Lab Vac, Sigma-Aldrich). The spinach leaves (at least 6), which petiole was removed using a sharp scalpel, were immersed in the impregnating solution during the entire procedure. Based on preliminary experiments to establish maximum weight gain and avoiding tissue damage of spinach, a two cycles, stepwise protocol with a minimum absolute pressure of 150 mbar was chosen (also referred as mild vacuum protocol in this paper). The value of the apparent porosity was used as a reference value for understanding the maximum levels of weight gain that could be achieved (Tylewicz et al., 2012). During vacuum impregnation, the pressure gradually decreased from the atmospheric value (1000 mbar) to the final reduced pressure value (150 mbar) in 10 min. The pressure was kept at 150 mbar for 2 min before releasing the vacuum and letting the pressure to progressively return to the atmospheric value in 10 min. This impregnation cycle was repeated once more to ensure maximum weight gain.

In a separate experiment, aiming at achieving partial impregnation of the leaf samples (also referred as low vacuum protocol in this paper), the pressure gradually decreased from the atmospheric value to a reduced pressure value of 300 mbar in 7.5 min. When vacuum was released, the pressure progressively returned to the atmospheric value in 8.5 min.

After impregnation, the leaf samples were gently blotted with tissue and weighed to determine their weight gain. For μCT, samples from leaves totally or partially impregnated in the trehalose solution and two controls (non-impregnated leaves and leaves kept in the impregnating solution overnight (no vacuum)) were prepared.

### 2.5. X-ray computed tomography (CT)

#### 2.5.1. Sample preparation

After weighing, leaves (3 per each treatment) were placed in a closed Petri dish in which a tissue wet in distilled water was previously placed for saturation. Each leaf was placed on a polystyrene foam mounting stage with the upper surface in contact with the stage. A layer of Parafilm® was gently wrapped around the lower surface of the sample and the stage to avoid sample dehydration and to keep the sample in a vertical position during the scan (Fig. 1).

#### 2.5.2. Scanning

The samples were scanned within 15 min after completing the vacuum impregnation procedure. Each leaf was scanned using an X-ray CT system (Tomohawk, AEA Technology, UK) using an X-ray source Philips HOMX 161 (Philips Medical Systems Gmbh, Hamburg, Germany) at a voltage of 70 kV and current of 0.5 mA. A 2-mm aluminum filter was placed before the detector to increase

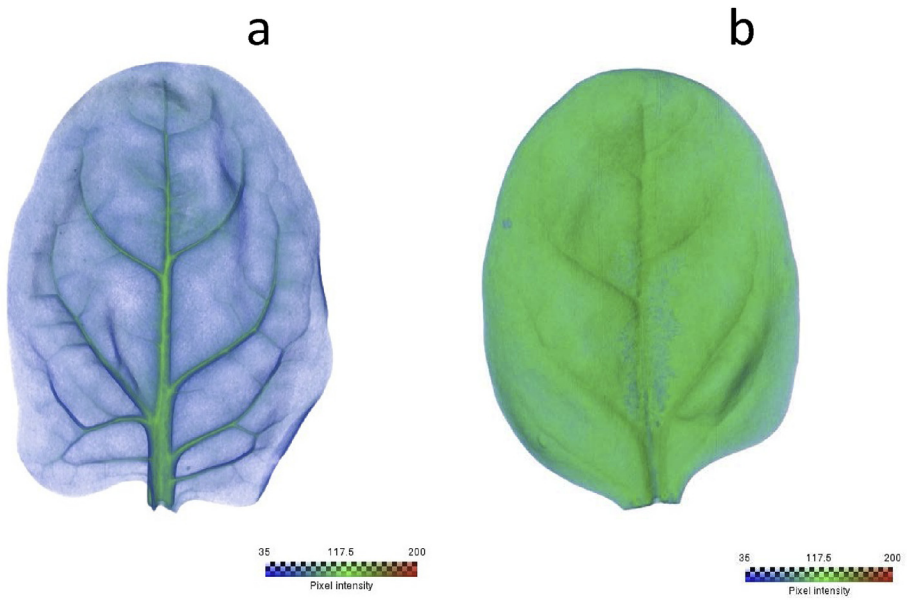


**Fig. 1.** Typical result of volume rendering of leaves obtained with X-ray CT. Non-impregnated tissue is represented blue, veins and impregnated tissue are represented green. (a) untreated control (b) trehalose-treated leaf. (For interpretation of the references to colour in this figure legend, the reader is referred to the web version of this article.)

the signal-to-noise ratio. Each pixel in final image represented a linear resolution of 55 μm. Frame averaging of 32 images and an angular increment of 0.5° were used in a scan over 187°. The scanning procedure lasted 25 min.

The X-ray shadow projections of the leaf were processed by a mathematical algorithm based on the back-projection procedure (Tomohawk software version 3.5.2, AEA Technology, UK) to obtain reconstructed cross-sectional gray scale images of the attenuation coefficient of the tissue.

The SkyScan NRecon software (Bruker, Belgium) was used to reconstruct cross-sectional images, correcting for beam hardening and ring artefacts. Adjustment of misalignment was also performed.

#### 2.5.3. Processing and volume rendering

The reconstructed images were loaded into the Avizo Fire Edition software 7.0.1 (VSG, Bordeaux, France) and segmented into spinach tissue and air. Otsu's algorithm was applied for optimal thresholding (Musse et al., 2010; Pareyt et al., 2009). The threshold values calculated with Otsu's algorithm were $34 \pm 1$ and $56 \pm 1$ for respectively untreated and trehalose impregnated leaves (8-bit images). A threshold value of 35 was chosen and applied to all the reconstructed images (background range = 0–35; object range 35–255). The binary images were filtered for small isolated pixels.

A 3D surface was generated to describe the geometric information of the leaf. The grey scale is visualised in the 3D surfaces by using colours (low values are blue; middle values are green; high values are red).

### 2.6. X-ray computed micro tomography (μCT)

#### 2.6.1. Sample preparation

After weighing, leaves were placed in a closed Petri dish in which a tissue wetted with distilled water was previously placed for saturation. Leaves were taken out of the Petri dish and rectangular samples of the lamina (5 × 5 mm) were removed from three different positions with a microtome blade. The parts of the leaf that were sampled were previously determined based on the results obtained from the CT images obtained with the procedure described above, representing different areas of the leaf where different impregnation characteristics were expected.

#### 2.6.2. Scanning

The samples were scanned using a SkyScan1172 high-resolution X-ray micro-CT system (Bruker, microCT, Kontich, Belgium), operating a 60 keV, a rather low X-ray energy well suited for scanning soft, biological materials. The experimental conditions were optimized to obtain high-quality radiographic projection images, while considering the contrast and resolution, as well as manageable scanning times (15 min per sample). The X-ray shadow projections of the 3D object were digitalized as 2000 × 1048 pixel images, which were processed to obtain reconstructed cross-sectional images using a mathematical algorithm based on the filtered back-projection procedure implemented in the NRecon 1.6.2.0 software (Skyscan, Belgium). This resulted in a 3D stack of 950 virtual sections, each consisting of 1244 × 344 isotropic voxels (= $4.8^3$ $\mu m^3$), with a linear X-ray attenuation coefficient displayed as a grey scale value calibrated between 0 and 255.

#### 2.6.3. Segmentation

The images were processed using the Skyscan CTAn software (Bruker, microCT, Kontich, Belgium). To define a global threshold value for segmenting air paces from tissue, Otsu's alghorithm was applied on datasets of controls and impregnated samples. In the untreated samples the histograms of grey level frequencies obtained were monomodal, while in impregnated samples the histograms were bimodal distributed. Otsu's alghorithm works better on bimodal distributed histograms and 49 was the chosen threshold because it was the lowest obtained among the impregnated samples. This threshold value was applied to all the dataset recorded.

In order to exclude the damaged cells as a result of the cutting of the sample, the image datasets were trimmed removing about 100 pixels (0.5 mm) from each cut edge.

#### 2.6.4. Morphometric analysis

The following morphometric parameters were quantified:

- Total, open and closed porosity (%), quantified as a fraction of the total volume of the sample by applying 2D and 3D algorithms (Herremans et al., 2013).
- Stomata density, quantified as the number of stomata per leaf square millimetre by obtaining a 1.5 mm × 1.5 mm leaf subsample, segmenting the void spaces then applying the autoskeleton module on Avizo 9 (FEI, Oregon, USA) to the void network to extract the essential geometry. Networks extending beyond the leaf surface due to open stomata was counted and reported.
- Pore thickness distribution (μm), defined as the average thickness of the pores. This parameter is calculated by skeletonization of the binarised tissue image followed by a sphere fitting algorithm for each voxel of the skeleton (Hildebrand and Rìegsegger, 1997).

#### 2.6.5. Surface rendering

To better highlight the contrast between tissue and pores, surface rendering of the binary images was performed. A mesh was created by wrapping the tissue surface. Since the process of surface rendering is computationally demanding, the images were cropped and the surface rendering was only applied on a portion of the sample (300 pixels × 300 pixels = 1.5 mm × 1.5 mm). This portion is normally selected in the centre of the sample.

### 2.7. Statistical analysis

Statistical significance ($p < 0.05$) of the treatments was tested by means of one-way ANOVA analysis using MS Excel (Microsoft Corp., Redmond, WA, USA). The Tukey–Kramer multiple comparison test was used to analyse differences between treatments.

## 3. Results

### 3.1. Apparent porosity and weight gain after VI

The real solid-liquid density ($\rho_r$) was 1.167 ± 0.081 and the apparent density ($\rho_a$) was 0.710 ± 0.021. The effective porosity of the spinach leaf was calculated from Equation (1) and the result was 39 ± 4%. This value of apparent porosity was used as a reference value for understanding the levels of weight gain that could be achieved with the VI protocol (Tylewicz et al., 2012). In the case of the spinach leaves, this protocol provoked a weight gain ranging from 39 to 50%.

### 3.2. Visualization of leaf impregnation by X-ray CT

Fig. 1 shows the results of the volume rendering of the control and trehalose-impregnated samples using the mild vacuum protocol. In the control samples, the leaf tissue is blue while the veins are green. In the impregnated samples, impregnated tissue is show in green.

Fig. 1b shows that the edges of the impregnated leaf as well as some areas around the main vein have lower pixel intensity, appearing blue in the figure. This result suggests uneven impregnation of the trehalose solution in the leaf and, therefore, three samples in different positions in the leaf were obtained for a more detailed analysis in the X-ray μCT. Fig. 2 shows the sampling points.

In the figure, “position 1” refers to a sample taken 15 mm from the upper edge of the leaf and 5 mm from the main vein; the x-ray CT shows this position without any blue area. “Position 2” refers to a sample taken in the centre of the leaf, close to the main vein; the X-ray CT shows areas of blue colour in this position. “Position 3” refers to samples taken by the lower edge of the leaf, close to the main vein.

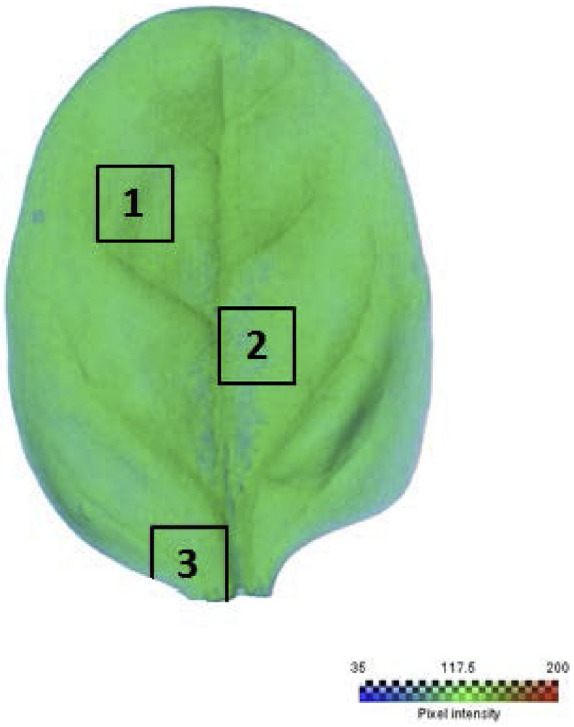


**Fig. 2.** Schematic of the sampling performed on trehalose impregnated spinach leaves for X-ray μCT scanning.

### 3.3. Visualization of leaf impregnation by X-ray μCT

Fig. 3 reports typical results of reconstructed leaf cross sections (2D and 3D) after scanning with X-ray μCT. In Fig. 3A, the cross-section of the untreated leaf (position 1) reveals recognizable structures: upper and lower epidermis, palisade mesophyll, spongy mesophyll, veins and the air surrounding the different cell structures. After partial impregnation, the remaining air space seems to be distributed mostly around the palisade mesophyll (Fig. 3B). Overnight dipping in the trehalose solution (Fig. 3C) seems to distribute the solution evenly in the cross section of the leaf. In Fig. 3D, the cross-section of the leaf (position 1) has been filled up by the trehalose solution during the mild vacuum impregnation protocol although small pockets of air are still distinguishable. Bright spots in the cross section might be due to the presence of calcium oxalate crystals (Biel et al., 2010).

### 3.4. Porosity and stomata density

Fig. 4 shows the average porosity of the samples in each of the studied positions in the leaf. Untreated leaves show porosity values of around 48% of the total volume, which is slightly higher than the value obtained with the pycnometer method. The partial impregnation treatment leads to a leaf porosity value lower than the untreated sample but higher than the other impregnation treatments. The mild-vacuum impregnation treatment as well as the overnight dipping treatment reduces the porosity value about ten times without significantly differences between their values of final porosity. The porosity values of untreated leaves and mild-vacuum impregnated leaves are similar in the three positions while the partially impregnated leaves show a higher porosity in the edge.

Table 1 shows that the volume of closed pores represents less

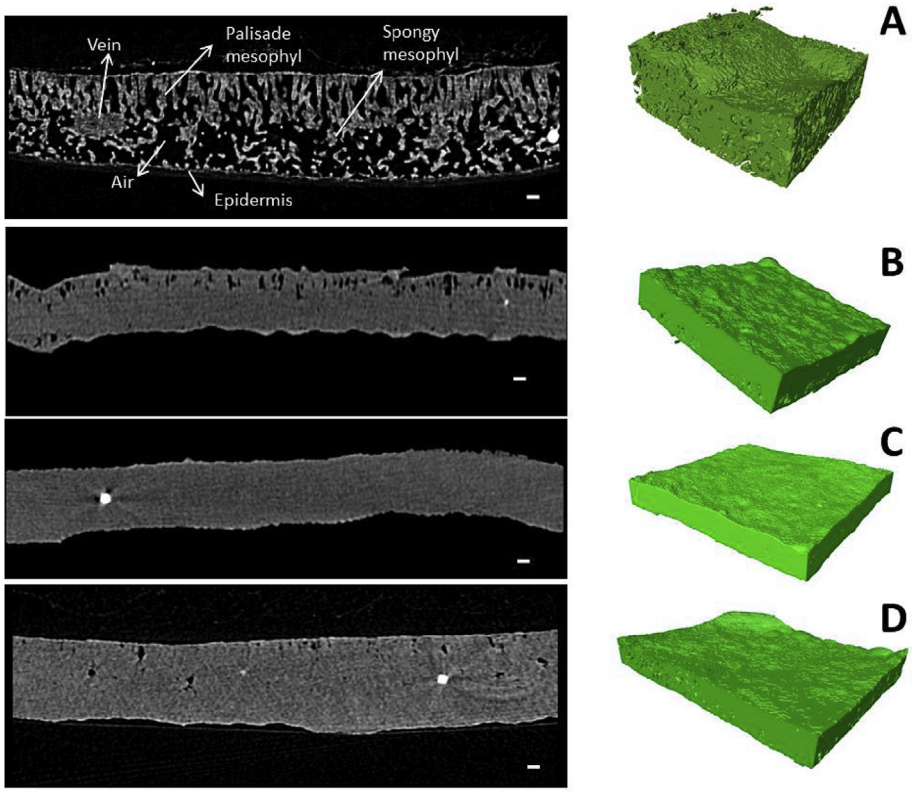


**Fig. 3.** Typical results from cross-section reconstruction of spinach leaves (position 1). (A) raw, untreated leaf where tissue structures and surrounding air are visible. (B) The leaf has been partially impregnated (low vacuum protocol) with an isotonic trehalose solution. Pockets of air are visible mostly around the palisade mesophyll. (C) Leaves were dipped in isotonic trehalose solution overnight. (D) The leaf was vacuum impregnated (high vacuum protocol) with an isotonic trehalose solution. Few air pockets are still visible. *Left panel*: 2D reconstruction of the leaves, scale bar = 100 μm. *Right panel*: 3D reconstructed images of leaves using surface rendering.

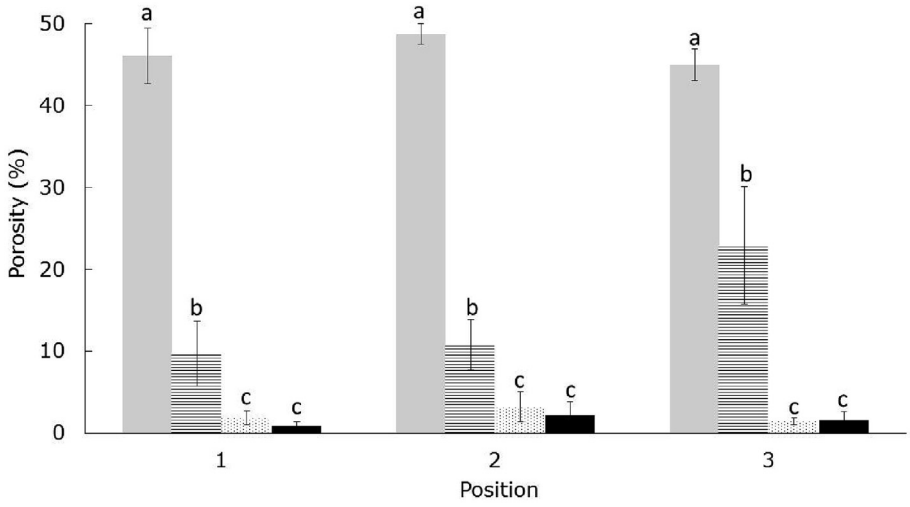


**Fig. 4.** Average total porosity of spinach of three samples of baby spinach leaves obtained in different positions in the leaf as indicated in the Materials and methods section. Average and standard deviation from at least three replicates are reported. Grey-filled bar: untreated sample, line-filled bar: partially impregnated sample, dotted bar: sample dipped in trehalose overnight, black-filled bar: fully impregnated tissue. Letters above the error bars indicate statistical differences ($p < 0.05$).

**Table 1**
Porosity and stomata density of untreated spinach leaves. Reported is the average and standard error of the measurements in the three studied positions in the leaves.

| Leaf volume ($mm^3$) | Total porosity (%) | Open porosity (%) | Closed porosity (%) | Stomata/$mm^2$ (upper surface) | Stomata/$mm^2$ (lower surface) |
|---|---|---|---|---|---|
| 7.77 ± 0.72 | 49.23 ± 1.56 | 49.17 ± 1.57 | 0.06 ± 0.01 | 13.39 ± 4.31 | 53.72 ± 14.41 |

than 0.1% of the total porosity of the leaf and that stomatal density is higher on the bottom part of the leaf than at the top. The stomatal distribution is illustrated in Fig. 5.

### 3.5. Porosity distribution

The pore thickness distribution of the analysed samples is reported in Fig. 6, where it is clearly shown that larger pores are easily filled by the solution. In the untreated sample (Fig. 6A), the peak of pore thickness distribution is close to 20 μm in the three analysed positions. In the impregnated samples (Fig. 6B–D), the proportion of large pores (>100 μm) decreased drastically while the proportion of small pores (<50 μm) increased in around 100%. Both partial and total vacuum impregnated tissue drastically increased the proportion of pores with 10 μm diameter, an increase that is less pronounced when the leaves were dipped in the trehalose solution overnight.

## 4. Discussion

The observations and microstructural measures that were produced in this study can be used to help explaining certain mechanisms of vacuum impregnation of baby spinach leaves. The majority of the intercellular air fraction is located in the spongy mesophyll (Warmbrodt and Woude, 1990), which might be more easily replaced by the trehalose solution than the air around the palisade, as suggested by the partial impregnation test (Fig. 3B). As the volume of closed pores in the palisade is much lower than the remaining porosity after impregnation (less than 0.1% compared with a total remaining porosity of around 1%), we suggest that the impregnation of the palisade is strongly influenced by the stomatal density at the surface of the leaf. Higher stomatal density at the lower leaf surface provides easier access for the impregnating solution to the pores below the epidermis as compared to the upper leaf surface. Dymek et al. (2014, 2015) showed that stomata remain open after vacuum impregnation, suggesting that they are not flooded with solution after the impregnation process as they would close if flooded (Sibbernsen and Mott, 2010). With μCT it was only possible to view the open stomata on the fresh leaf samples.

Porosity results suggest that impregnation of the edge is more difficult above a certain threshold of operating conditions (Fig. 4). Pressure thresholds leading to pore impregnation have been shown to be tissue dependent (Panarese et al., 2013), probably reflecting differences in the porous structure in different sections of the leaf. Furthermore, it is clearly shown that, under the experimental conditions tested in this work, complete pore impregnation was not

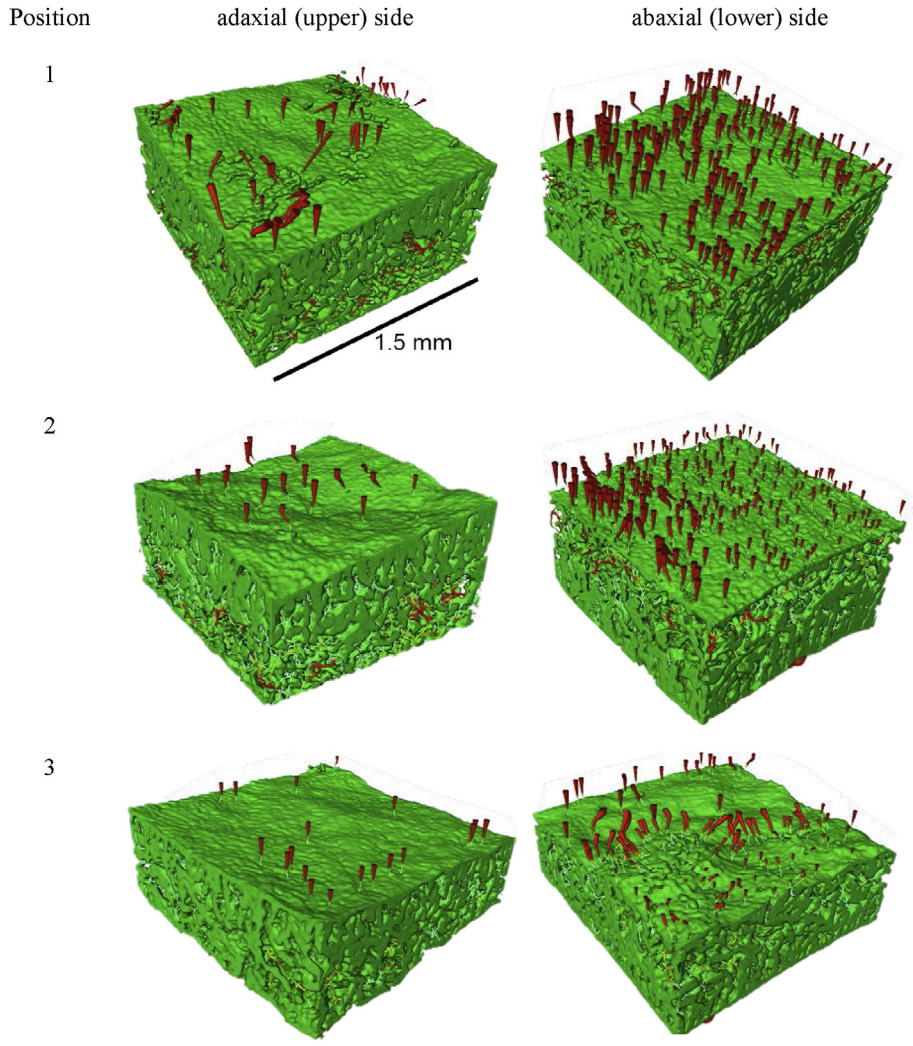


**Fig. 5.** Identification (red symbols) of the stomata on two sides and at different positions (see Fig. 2) of baby spinach leaves after skeletonization of the pore network. (For interpretation of the references to colour in this figure legend, the reader is referred to the web version of this article.)

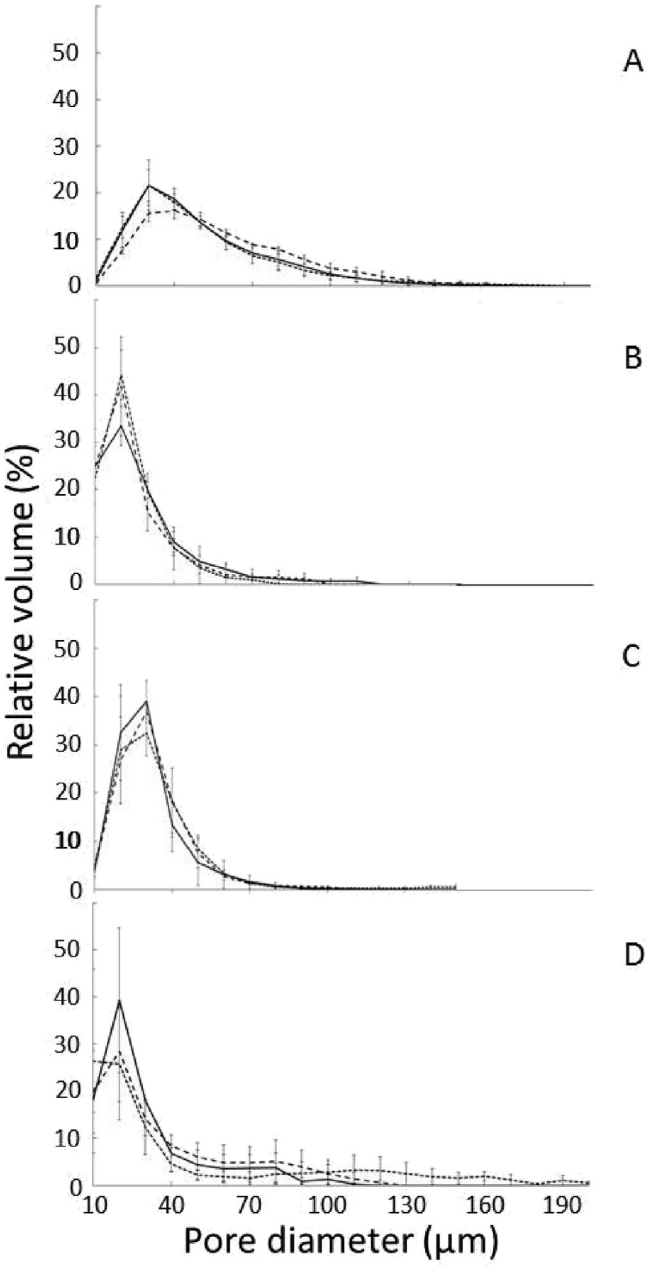


**Fig. 6.** Pore thickness distribution of three samples of baby spinach leaves obtained in different positions in the leaf as indicated in the Materials and methods section. (→ →) position 1; (– –) position 2, (–) position 3. (A) untreated control, (B) partially impregnated with isotonic trehalose solution, (C) samples were dipped in isotonic trehalose solution overnight, (D) impregnated with isotonic trehalose solution. Average and standard deviation from at least three replicates are reported.

possible (Fig. 5). As a consequence, the leaves are still metabolically active and respire (data not shown). Panarese et al. (2014) using a similar VI protocol, reported an increase of metabolic activity in baby spinach leaves that could be explained by the utilization of mitochondrial oxygen consuming pathways. Photorespiration was also proved to continue in the impregnated leaves, which could be attributed to the air present in the remaining porosity, as dissolved oxygen in the solution is very low and its diffusion too slow to support respiration.

## 5. Concluding remarks

X-ray micro tomography is a powerful tool for investigating the efficiency of vacuum impregnation protocols as well as the influence of structural characteristics of the tissue on the impregnation process. Our results reveal that the area around the spongy mesophyll is easier impregnated than the area around the palisade mesophyll. The impregnation of the palisade is strongly influenced by the stomatal density at the surface of the leaf. The low vacuum impregnation protocol applied here provoked less impregnation close to the edge of the leaf than in its centre, probably accounting for an influence of the tissue structure on impregnation. The mild vacuum impregnation protocol tested in this investigation, which was designed on the basis of measured apparent porosity, does not achieve full impregnation of the tissue and small pores (<50 μm) are still found.

VI has broad applications in fruit and vegetable processing and it is, therefore, essential to determine the appropriate parameters to ensure the desired effects on tissue properties and/or processability. Microtomography provides a powerful mean of improving our understanding of the impregnation process dynamics which is a key issue for process optimization.

## Acknowledgements

V. Panarese acknowledges the financial support from the Portuguese Foundation of Science (FCT). F. Gãmez Galindo acknowledges the financial support from European Community's Seventh Framework Program (FP7/2007-2013) under grant agreement no. 245280, also known under the acronym PRESERF. Financial support of FWO Vlaanderen (project G.0645.13), the Flemish government agency for Innovation by Science and Technology (project IWT SBO120033 TomFood) and the University of Leuven (project OT 12/055) is gratefully acknowledged. Dennis Cantre is an IRO scholar of KU Leuven. We also acknowledge the Hercules foundation for supporting the X-ray CT facility (AKUL001(HER/09/016)).

## References

Barrera, C., Betoret, N., Corell, P., Fito, P., 2009. Effect of osmotic dehydration on the stabilization of calcium-fortified apple slices (var. Granny Smith): influence of operating variables on process kinetics and compositional changes. J. Food Eng. 92, 416–424.

Biel, K.Y., Fomina, I.R., Nazarova, G.N., Soukhovolsky, V.G., Khlebopros, R.G., Nishio, J.N., 2010. Untangling metabolic and spatial interactions of stress tolerance in plants. 1. Patterns of carbon metabolism within leaves. Protoplasma 245, 49–73.

Carciofi, B.A.N., Prat, M., Laurindo, J.B., 2012. Dynamics of vacuum impregnation of apples: experimental data and simulation results using a VOF model. J. Food Eng. 113, 337–343.

Dymek, K., Dejmek, P., Gãmez Galindo, F., 2014. Influence of pulsed electric field protocols on the reversible permeabilization of rucola leaves. Food Bioprocess Technol. 7, 761–773.

Dymek, K., Retelj, L., Zorec, B., Pavšelj, N., Dejmek, P., Gãmez Galindo, F., Miklavčič, D., 2015. Modeling electroporation of the non-treated and vacuum impregnated heterogeneous tissue of spinach leaves. Innov. Food Sci. Emerg. Technol. 29, 55–64.

Fito, P., 1994. Modelling of vacuum osmotic dehydration of foods. J. Food Eng. 27, 229–240.

Fito, P., Pastor, R., 1994. Non-diffusional mechanisms occurring during vacuum osmotic dehydration. J. Food Eng. 21, 513–519.

Fito, P., Andrés, A., Chiralt, A., Pardo, P., 1996. Coupling of hydrodynamic mechanism and deformation–relaxation phenomena during vacuum treatments in solid porous food–liquid systems. J. Food Eng. 27, 229–240.

Fito, P., Chiralt, A., 2000. Vacuum impregnation of plant tissues. In: Alzamora, S.M., Tapia, M.S., Lãpez-Malo, A. (Eds.), Minimally Processed Fruits and Vegetables: Fundamental Aspects and Applications. Springer, Berlin, pp. 189–202.

Gras, M., Vidal-Brotãns, D., Betoret, N., Chiralt, A., Fito, P., 2002. The response of some vegetables to vacuum impregnation. Innov. Food Sci. Emerg. Technol. 3, 263–269.

Gras, M.L., Vidal, D., Betoret, N., Chiralt, A., Fito, P., 2003. Calcium fortification of vegetables by vacuum impregnation. Interactions with cellular matrix. J. Food Eng. 56, 279–284.

Herremans, E., Verboven, P., Bongaers, E., Estrade, P., Verlinden, B., Wevers, M., Nicolai, B., 2013. Isolation of single cells and pores for the characterisation of 3D fruit tissue microstructure based on X-ray micro-CT image analysis. In: Proceedings of InsideFood Symposium, Leuven, Belgium.

Hildebrand, T., Rìegsegger, P., 1997. A new method for the model-independent assessment of thickness in three-dimensional images. J. Microsc. 185, 67–75.

Hironaka, K., Kikuchi, M., Koaze, H., Sato, T., Kojima, M., Yamamoto, et al., 2011. Ascorbic acid enrichment of whole potato tuber by vacuum-impregnation. Food Chem. 127, 1114–1118.

Lozano, J.E., Rotstein, E., Urbicain, M.J., 1980. Total porosity and open-pore porosity in the drying of fruits. J. Food Sci. 45, 1403–1407.

Musse, M., De Guio, F., Quellec, S., Cambert, M., Challois, S., Davenel, A., 2010. Quantification of microporosity in fruit by MRI at various magnetic fields: comparison with X-ray microtomography. Magn. Reson. Imaging 28, 1525–1534.

Panarese, V., Dejmek, P., Rocculi, P., Gãmez Galindo, F., 2013. Microscopic studies providing insight into the mechanisms of mass transfer in vacuum impregnation. Innov. Food Sci. Emerg. Technol. 18, 169–176.

Panarese, V., Rocculi, P., Baldi, E., Wadsæ, L., Rasmusson, A.G., Gãmez Galindo, F., 2014. Vacuum impregnation modulates the metabolic activity of spinach leaves. Innov. Food Sci. Emerg. Technol. 26, 286–293.

Pareyt, B., Talhaoui, F., Kerckhofs, G., Brijs, K., Goesaert, H., Wevers, M., et al., 2009. The role of sugar and fat in sugar-snap cookies: structural and textural properties. J. Food Eng. 90, 400–408.

Phoon, P.Y., Gãmez Galindo, F., Vicente, A., Dejmek, P., 2008. Pulsed electric field in combination with vacuum impregnation with trehalose improves the freezing tolerance of spinach leaves. J. Food Eng. 88, 144–148.

Salvatori, D., Andrés, A., Chiralt, A., Fito, P., 1997. The response of some properties of fruit to vacuum impregnation. J. Food Process Eng. 21, 59–73.

Schulze, B., Peth, S., Hubbermann, E.M., Schwarz, K., 2012. The influence of vacuum impregnation on the fortification of apple parenchyma with quercetin derivatives in combination with pore structures X-ray analysis. J. Food Eng. 109, 380–387.

Sibbernsen, E., Mott, K.A., 2010. Stomatal responses to flooding of the intercellular air spaces suggest a vapor-phase signal between themesophyll and the guard cells. Plant Physiol. 153, 1435–1442.

Tylewicz, U., Lundin, P., Cocola, L., Dymek, K., Rocculi, P., Svanberg, S., et al., 2012. Gas in scattering media absorption spectroscopy (GASMAS) detected persistent vacuum in apple tissue after vacuum impregnation. Food Biophys. 7, 28–34.

Tylewicz, U., Romani, S., Widell, S., Gãmez Galindo, F., 2013. Induction of vesicle formation by exposing apple tissue to vacuum impregnation. Food Bioprocess Technol. 6, 1099–1104.

Verboven, P., Herremans, E., Helfen, L., Ho, Q., Abera, M., Baumbach, T., Wevers, M., Nicolai, B., 2015. Synchrotron X-ray computed laminography of the three dimensional anatomy of tomato leaves. Plant J. 81, 169–182.

Warmbrodt, R.D., Woude, W.J.V., 1990. Leaf of Spinacia oleracea (Spinach). Ultrastructure, and plasmodesmatal distribution and frequency, in relation to sieve-tube loading. Am. J. Bot. 77, 1361–1377.